HYDRODYNAMICS OF THE WALL LAYER IN A CUBIC-PACKING MODEL

V. I. Volkov, N. S. Danilov, V. D. Zhak,
V. A. Mukhin, V. E. Nakoryakov, V. I. Titkov,
and Ya. Ya. Tomsons

UDC 532.546.6

Although there are many papers on the hydrodynamics of flows in porous media, there is still a lively discussion on the details of the flow [1-5]. For example, doubt has been cast on the existence of stagnant zones between particles, and conflicting views have been put forward on the velocity profile near the wall [2, 3].

There are conflicting viewpoints on the detailed hydrodynamic picture because there are no direct measurements on the velocity profile within porous media with transducers sensitive to flow direction.

There are a few experimental studies on the velocity profiles within porous media with thermoanemometer and electrochemical transducers [2-4]. Measurements with such transducers are made in free spaces having transverse dimensions of 0.1-0.2 times the diameter of the sphere, which in the models on average did not exceed 1 cm. This explains the difficulty in making measurements with contact transducers and the impossibility of making measurements with a crossed-filament thermoanemometer, because of the large size. Also, the readings of thermoanemometers and electrochemical transducers are distorted near the wall, and it is difficult to correct for this effect, since the distance from the transducer to the wall of a sphere is unpredictable in a random packing, while the flow direction within the pores is also unknown. In such flows, the readout from a thermoanemometer or electrochemical transducer is due to the modulus of the velocity. Therefore, there is some doubt over the data on the velocity profiles within beds. Also, there are the design difficulties in measuring the velocity vector with a contact transducer within a porous medium, so it is unlikely that the actual hydrodynamic picture within a porous medium will be known within the near future.

There are difficulties due to the natural complexity in using velocity-measurement methods such as laser Doppler devices, e.g., deviation of the beam from any curvilinear surface.

These laser devices have been used to measure the liquid speed between spheres constituting a model for a porous medium, with avoidance of the deviation from curvilinear surfaces by the choice of the liquid whose refractive index is equal to that of the glass spheres.

Various LDVM schemes have been described with detailed modes of operation [6-8].

The experiments were performed with two optical systems capable of operating with sign-varying flows. A differential scheme provided sensitivity to flow direction by the use of two Doppler signals displaced in phase by $+\pi/2$ or $-\pi/2$ in accordance with the direction of motion. In the system with a reference beam and Bragg cell, use was made of the frequency shift at a high frequency f_0, which was added to or subtracted from the Doppler frequency (Fig. 1). The working principles of both systems have been examined in detail [6-8], and therefore here we consider only the main features.

In determining the sign velocity with a differential scheme it was found that complete subtraction of the additive component was practically impossible on account of the partial depolarization at the mirrors, particles, and so on. Also, it was difficult to realize identity for all three beams at the photomultiplier.

Therefore, there were large distortions after the differential amplifier, particularly when the noise and Doppler spectra overlapped near zero in the case of backward flows. Subsequently, the differential scheme was used to determine the modulus of the longitudinal component of the velocity, and the basic measurements were made in the narrowest sections of the packing, in which one can guarantee the absence of reverse flows. The measurements with the differential optical scheme involved deviation from a single-mode spectrum for the Doppler signal. For example, the spectrum became bimodal as the measurement volume approached the spheres, i.e., there were two Doppler frequencies differing by a factor two. The stable position of the spectra meant that the bimodal spectrum could not be explained by the coherent effects reported in [6]. It may be that scattering when the beam contacted a sphere resulted in the reference-beam mode occurring at the same time as the differential scheme, and this has half the angle of convergence of the rays. As the velocity increased, the Doppler-signal spectrum showed combination frequencies in the ratio 1:2:4 for Re of about 400 and above (here Re was derived from the flow speed in the narrow section and the diameter of a sphere), while there were others in the ratio 3:5:7, while the value of the Doppler frequency did not remain constant, which resulted in overlap between the spectra of the individual frequencies,

Translated from Zhurnal Prikladnoi Mekhaniki Tekhnicheskoi Fiziki, No. 6, pp. 58-64, November-December, 1980. Original article submitted January 10, 1980.

0021-8944/80/2106-0786$07.50

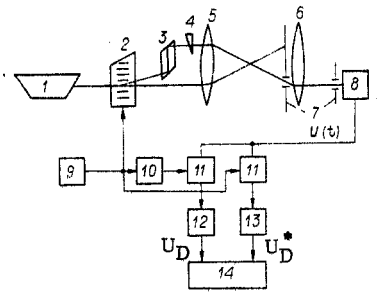

Fig. 1

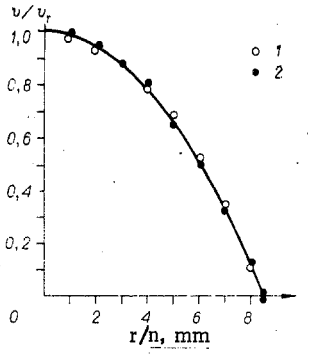

Fig. 2

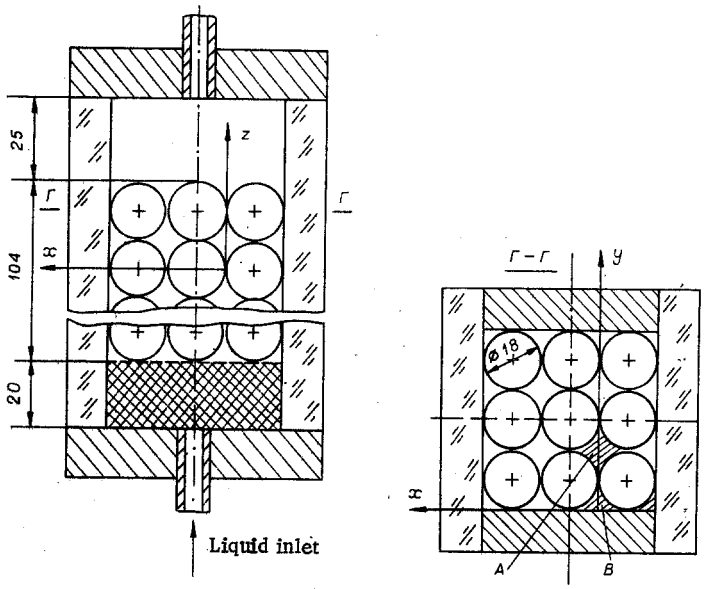

Fig. 3

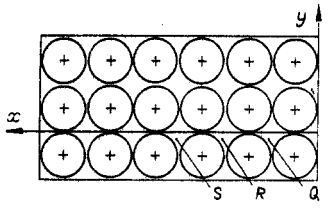

Fig. 4

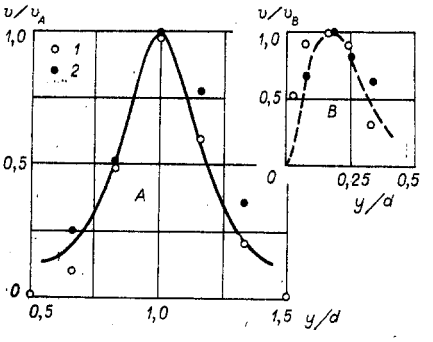

Fig. 5

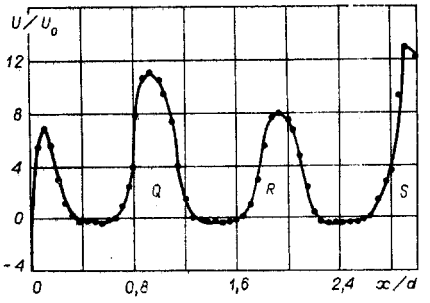

Fig. 6

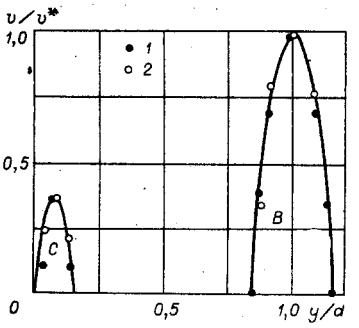

Fig. 7

and it became virtually impossible to identify the Doppler frequency with the differential system above Re $\sim$ 400.

A radical solution on the noise, particularly the additive component, is provided by an optical scheme with frequency shift for one of the beams [6-8]. Figure 1 shows such a scheme with a reference beam and Bragg cell. The laser 1 works with the Bragg cell 2, prism 3, optical wedge 4, focusing lens 5, stop 7, receiving lens 6, photomultiplier 8, high-frequency generator 9, phase shifter 10, mixers 11, low-pass filters LPF1 12 and LPF2 13, and tracking filter 14. The signal from the last passes to the spectrum analyzer. Then the signal at the output of the photomultiplier is

$$U(t) = B(t) + A(t) \sin (2\pi f_0 + \mathbf{kv}_D)t,$$

where k and v_D are the wave vector and flow speed. This signal can be represented ideally as two orthogonal Doppler signals if the passband ω_{LPF} for LPF1 and LPF2 is chosen such that

$$\omega_{LPF} < \omega_0, \quad \omega_0 - \omega_u < \omega_{LDF}$$

where $\omega_0 = 2\pi f_0$ and ω_u is the upper frequency of the additive component, by which is meant the signal frequency not exceeding a given level. The following signals then appear at the output of LPF1 and LPF2:

$$U_D = K_f A(t) \sin (\mathbf{kv}_D t + \varphi_{LDF}), \qquad U_D^* = K_f A(t) \cos (\mathbf{kv}_D t + \varphi_{LDF}).$$

The filters are assumed to be identical with flat frequency response. To measure the Doppler signal represented by the two orthogonal terms one employs the tracking filter, which provides for simultaneous measurement and recording of the Doppler frequency, the velocity, and the flow direction. The tracking filter can work in spectrum analyzer mode to locate the signal and lock onto it, and also to monitor the tracking. An advantage of this device is that one measures the absolute values of the Doppler frequency with the signs.

This system can measure small Doppler shifts (about ± 1 Hz) and large ones (in this instrument, the maximum frequency range was ± 2.4 MHz, which is not the limit.

The operation of the optical system was checked by measuring a standard profile in a cylindrical glass tube. Figure 2 shows the results, where r/n is the ratio of the radius of the tube to the refractive index of the liquid and v/v_T is the ratio of the current velocity to the maximum value. The measurements were made at a distance of 30 tube diameters from the inlet with Re of 400 and 200 (points 1 and 2 respectively), as deduced from the flow velocity and the tube diameter. The solid line shows the theoretical profile. The error of measurement of the parabolic profile was not more than 5%. The error was more substantial in measuring the velocity profile between the spheres (Figs. 3 and 4), and the reproducibility of the results was then about 10%. The measured flow speed agreed with that calculated from the flow rate within the same error limits. This discrepancy is related to the measurement of low speeds in the presence of a velocity gradient.

It was found that the error of measurement in the packing of glass spheres was dependent also on the temperature stabilization of the working loop, as well as on the purity of the liquid and the cleanness of the spheres. If the spheres were coated with a thin film of deposit, there was practically no deviation in the laser beam, but large distortions arose on account of recording of luminescent points on the surface.

The measurements with the differential scheme were made with the working section shown in Fig. 3. This had a regular packing of six layers of spheres of diameter 18 mm. Each layer contained nine spheres. The nonuniformity in the flow at the input was eliminated by a layer of 2-mm spheres of thickness about 2 cm.

The system with the reference beam and Bragg cell was used in measuring the flow speed in the working part shown in Fig. 4. Here there were 16 layers of spheres regularly packed with 18 spheres in each layer. The measurements were made in the wide section after the eighth layer.

A cubic-packing model was chosen primarily because the wall region in a real porous bed made of spheres usually corresponds to regular cubic packing [1].

Figures 5 and 6 show the results. Figure 5 shows the observed velocities as related to the maximum values v_A (region A) and v_B (region B) in the narrow section of the channel as a function of the transverse coordinate y/d, where d is the diameter of the sphere and v_A and v_B were respectively 20.4 and 9.1 mm/sec for Re = 120 (point 1) and 43.6, or 24.5 mm/sec for Re = 300 (point 2). The measurements were made on the working part as shown in Fig. 3 in the section x = 0, z = 0.

The measured velocity profiles can be related naturally to the theoretical velocity distributions for axially symmetrical flows (jet ones and in channels). The longitudinal component of velocity at the axis of such a jet varied by not more than 10%.

Therefore, the dependence on the longitudinal coordinate can be neglected to a first approximation. For qualitative comparison, we derived the scale of the transverse coordinate in the theoretical profile [9] by bringing the half-widths of the theoretical and observed profiles into coincidence. The solid lines in Fig. 5 show the results. The conversion scale in the wall cell was determined from equality of the transverse coordinates at the points of maximum velocity in the wall jet [9] and from the experimental profile. The broken line in Fig. 5 shows the theoretical velocity profile for a planar wall jet.

It is clear that the flow patterns in regions A and B do resemble jet flows. The jets are produced at the start of the packing and flow along the cylinders formed by the spheres, and they persist with small changes to a distance of about one sphere diameter after the bed. The velocity profile in cell A (Fig. 3) is not symmetrical with respect to the maximum value and differs from the profile in a jet, while the difference for Re = 300 is greater than that for Re = 120. This is obviously due to some detail of the packing and also to five layers of spheres being insufficient to standardize the flow. In the more highly obstructed sections of the channel, the velocity profiles also differ from jet ones and approximate to parabolic. For example, the solid line in Fig. 7 shows the parabola constructed from the maximum measured velocity. We also show the observed values of the longitudinal component of the velocity are referred to the maximum value (v^* = 29.1 and 7.5 mm/sec for Re of 300 and 200, points 1 and 2 respectively). The measurements were made near the wall of the channel (Fig. 3, z = 0, x/d = –0.87). Figure 7 shows that the velocity profile approximates to parabolic in the more obstructed parts, as distinct from the free parts, where jet flows predominate. The flow picture in the main remains unaltered as the number of spheres in the section increases, as Fig. 6 shows from the measured speeds referred to the flow-rate speed (v_0 = 3.23 mm/sec) in the wide section of the working part, in which one of the sides was increased by a factor two relative to the preceding working part. Figure 4 shows a section of this working part with the coordinate system. The measurements were made in the wide section of the channel unfilled with spheres. An improved optical system with a Bragg cell was used in the last part, which enabled us to detect backward flows, whose speed was up to 1/3 of the flow-rate speed and increased on moving from the wall of the channel to the center. This increase in speed in the backward flow may explain the observation that the speed between the second and third spheres (region R in Fig. 4 reckoned from the wall) was less than the speed between the first and second spheres or between the third and fourth ones (regions Q and S).

In conclusion we estimate the equivalent value Re_e for the jet in region A (Fig. 3): $Re_e = v_A d_e/\nu$, where $d_e = 0.27d$ is the equivalent diameter of region A and v_A is the flow-rate speed through region A. It can be shown that $Re_e \simeq 0.4$ Re, where Re is constructed from the flow speed in the narrow section of the channel and the sphere diameter.

Re_e did not exceed 160 in the experiments. Instability sets in a free jet at $Re_e \sim 15$ [9]. A constrained flow causes the onset of turbulence to shift to larger Re [5, 10]. In this model, the periodic restriction of the jet by the spheres shifted the onset of turbulence at least to $Re_e \sim 100$. At $Re_e \sim 160$ there was an increase in the velocity fluctuations, but it was impossible to establish whether this was due to increase in the flow instability or to perturbations from the inlet part.

In conclusion we note as follows:

1) a method has been developed for measuring the liquid speed in a porous medium by laser Doppler methods which involves equalizing the refractive indices of the porous medium and the liquid; and

2) these are the first measurements reported by a contactless method for measuring the velocity within a model for a porous bed composed of spheres.

LITERATURE CITED

1. M. É. Aérov, O. M. Todes, and D. A. Narinskii, Apparatus with Stationary Granular Beds [in Russian], Khimiya, Leningrad (1979).
2. E. J. Cairns and J. M. Prausnitz, "Velocity profiles in packed and fluidized beds," Ind. Eng. Chem., 51, No. 12 (1959).
3. V. A. Kirillov, V. A. Kuz'min, et al., "The velocity profile in an immobile granular bed," Dokl. Akad. Nauk SSSR, 245, No. 1 (1979).
4. H. S. Mickley, K. A. Smith, and E. J. Korchak, "Fluid flow in packed beds," Chem. Eng. Sci., 20, No. 3 (1965).
5. M. A. Gol'dshtik, "Theory of concentrated disperse systems," in: Proceedings of the International School on Transport Processes in Immobile Granular Beds [in Russian], Minsk (1977).
6. B. S. Rinkevichyus, Laser Anemometry [in Russian], Énergiya, Moscow (1978).
7. N. S. Danilov and V. I. Titkov, "A sign-sensitive laser anemometer," in: Algorithms for Processing and Automating Heat-Physics Experiments [in Russian], ITF SO AN SSSR, Novosibirsk (1978).
8. Yu. E. Nesterikhin (editor), Coherent-Optics Doppler Devices in Hydroaerodynamic Experiments [in Russian], Izd. Inst. Avtomat. Elektrometrii, Novosibirsk (1974).
9. L. A. Vulis and V. P. Kashkarov, Theory of Viscous-Liquid Jets [in Russian], Nauka, Moscow (1965).
10. B. I. Brounshtein and G. A. Fishbein, Hydrodynamics of Mass and Heat Transport in Dispersed Systems [in Russian], Khimiya, Leningrad (1977).